

# A new quantum propagator for hard sphere and cavity systems

J. Cao<sup>a)</sup> and B. J. Berne

Department of Chemistry, Columbia University, New York, New York 10027

(Received 10 March 1992; accepted 1 May 1992)

A new short time propagator for a particle interacting with a hard sphere or with a hard sphere cavity is derived. This new propagator is shown to be a much better approximation than the image approximations used in the literature and should prove useful for path integral or Green function Monte Carlo simulations. The simple example of the radial distribution function of a hard sphere gas is calculated using the new propagator as well as the older image approximation propagator and is shown to converge much more rapidly to the *ab initio* result.

## I. INTRODUCTION

The Feynman path integral offers a powerful tool for the study of quantum systems.<sup>1</sup> When the path integral is discretized the continuous paths are approximated by  $P$  segments on which the short time free particle propagator is used. The continuous path integral is then the  $P \rightarrow \infty$  limit of the discretized path integral. When hard boundaries are present, all paths must avoid the walls and convergence with  $P$  is extremely slow. Barker<sup>2</sup> provided a remedy for this slow convergence by introducing an image approximation, an approach that can be easily justified for rectangular boundaries, but which for curved boundaries is less justifiable. Image approximations to the propagator for hard spheres have been proposed and used in path integral simulations of hard sphere fluids. These are reasonable but it should be noted that they are based on a conjecture without any proof. Propagators based on the image approximation were first applied by Jacucci and Omerti<sup>3</sup> in their Monte Carlo calculation of the radial distribution of quantum hard spheres at finite temperatures. Later the same image approximation was used in the simulation of an excess electron in a hard sphere fluid<sup>4</sup> and the simulation of positronium in a hard sphere.<sup>5</sup> These were not the first applications of image approximations to treat hard spheres. In fact, earlier similar image approximations, suggested by Uhlenbeck and Beth,<sup>6</sup> were used by Whitlock and Kalos<sup>7</sup> in Green function Monte Carlo calculation of the radial distribution of quantum hard spheres.

In this paper we derive a new short time propagator for hard spheres based on the partial-wave expansion. This new short time propagator, although more complicated, is superior to the above image approximation propagator and Monte Carlo simulations based on it converge much more rapidly than simulations based on the image approximation propagator. The new propagator reduces to the image approximation under certain conditions. Thus it should be very useful in large scale simulations of quantum hard sphere liquids or electron solvation in classical hard sphere liquids.

We also derive the propagator for a particle inside a hard spherical box (or cavity). In this case a winding num-

ber has to be introduced. This is analogous to the case of a particle confined in a box. The result can also be reduced to the image approximation under the conditions. This new propagator can be used to study quantum particles in constrained geometries like pores. For example, one can study the electronic structure of atoms and molecules in cavities using this propagator.

The convergence properties of the new propagator is tested by using it in path integral Monte Carlo simulations of the second virial coefficient of quantum hard spheres and studying how fast it converges to "exact" *ab initio* calculations based on basic set expansions. We find that it converges much faster than similar Monte Carlo simulations based on the old image approximation.

## II. THE HARD SPHERE PROPAGATOR

The real time propagator,  $G(r, r', t)$ , of a quantum particle of mass  $m$  interacting with a hard sphere of radius  $a$  centered at the origin of the coordinate system depends on two length scales: the hard sphere radius  $a$  and a "wavelength"  $\lambda$  defined as

$$\lambda^2 = \frac{\hbar t}{m}, \quad (2.1)$$

in which  $t$  is the time. If  $\lambda \ll r, r', a$ , it will be possible to use a partial wave expansion to determine the real time propagator and by substitution,  $t \rightarrow -i\hbar\beta$ , the imaginary time propagator.

The wave-function basis set is taken to be the scattering wave solution of the hard sphere potential, that is

$$\psi_{\mathbf{k}}(\mathbf{r}) = e^{i\mathbf{k}\cdot\mathbf{r}} + \sum_{l=0}^{\infty} (2l+1) \times \sin(\delta_l) e^{i\delta_l} P_l[\cos(\chi)] \frac{e^{ikr}}{kr}, \quad (2.2)$$

where we assume the asymptotic partial wave formula at the large distance and where  $P_l$  is the Legendre function of the angle  $\chi$  formed by the two vectors  $\mathbf{k}$  and  $\mathbf{r}$ .  $e^{i\mathbf{k}\cdot\mathbf{r}}$  can be written as a Rayleigh expansion with the asymptotic expansion of the spherical Bessel functions as

<sup>a)</sup> In partial fulfillment of the Ph.D. in the Department of Physics, Columbia University.

$$e^{ikr} = e^{ix \cos(\chi)}$$

$$= \sum_{l=0}^{\infty} \frac{1}{2ix} [e^{ix} - (-1)^l e^{-ix}] (2l+1) P_l[\cos(\chi)], \tag{2.3}$$

where  $x = kr$  is a dimensionless variable. Substitution of this into Eq. (2.2) allows the wave function to be expressed as

$$\psi_k(\mathbf{r}) = \sum_{l=0}^{\infty} \frac{2l+1}{2ix} [e^{ix+2i\delta_l} - (-1)^l e^{-ix}] P_l(\cos \chi). \tag{2.4}$$

Now the propagator,  $G(\mathbf{r}, \mathbf{r}', t)$  from a space point  $\mathbf{r}$  to another point  $\mathbf{r}'$ , can be constructed

$$G(\mathbf{r}, \mathbf{r}', t) = \frac{1}{(2\pi)^3} \int d\mathbf{k} \psi_k^*(\mathbf{r}') e^{-i(\lambda k)^2/2} \psi_k(\mathbf{r}). \tag{2.5}$$

Insert Eq. (2.4) into Eq. (2.5) and integrate out the angular part we obtain

$$G(\mathbf{r}, \mathbf{r}', t) = \frac{1}{(2\pi)^3} \sum_{l=0}^{\infty} (4\pi)(2l+1) \times P_l[\cos(\chi)] \frac{1}{4rr'} I(r, r', l), \tag{2.6}$$

where  $\chi$  is the angle between the two vectors  $\mathbf{r}$  and  $\mathbf{r}'$ , and where  $I$  is the radial part and can be expressed as an integral

$$I(r, r', l) = \int_0^{\infty} dk e^{-i(\lambda k)^2/2} [e^{-ikr' - i2\delta_l} - (-1)^l e^{ikr'}] [e^{ikr + i2\delta_l} - (-1)^l e^{-ikr}]. \tag{2.7}$$

For a hard sphere of radius  $a$ , the phase shift is<sup>8</sup>

$$\delta_l = -(ka - \frac{l\pi}{2}) \tag{2.8}$$

if  $ka \gg 1$ . Thus the integral of  $k$  gives

$$I(r, r', l) = \sqrt{\frac{2\pi}{i\lambda}} [e^{i(r-r')^2/2\lambda^2} - e^{i(r-r'-2a)^2/2\lambda^2}]. \tag{2.9}$$

After rearranging the relevant terms in Eqs. (2.7) and (2.8), it follows that

$$\sum (2l+1) P_l[\cos(\chi)] \{e^{i(r-r')^2/2\lambda^2} - (-1)^l e^{i(r+r')^2/2\lambda^2} - [e^{i(u-2a)^2/2\lambda^2} - (-1)^l e^{iu^2/2\lambda^2}]\}, \tag{2.10}$$

in which  $u = (r+r')$ .

To transform back to the Cartesian coordinates, use can be made of relation Eq. (2.3). Then Eq. (2.10) can be reduced to

$$-2i \frac{rr'}{\lambda^2} e^{i(r-r')^2/2\lambda^2} + 2i \frac{a(u-a)}{\lambda^2} e^{iD/2\lambda^2}, \tag{2.11}$$

where

$$D = u^2 - 2au + 2a^2 - 2a(u-a) \cos(\chi). \tag{2.12}$$

Finally, putting all the pieces together, we find

$$G(\mathbf{r}, \mathbf{r}', t) = \left(\frac{1}{i2\pi\lambda^2}\right)^{3/2} \left[ e^{i(r-r')^2/2\lambda^2} - \frac{a(u-a)}{rr'} e^{iD/2\lambda^2} \right]. \tag{2.13}$$

The first term is obviously the free particle propagator, while the second term is due to the hard sphere. It satisfies the boundary condition, that is, whenever either of the space point is equal to the radius  $a$  of the sphere, the propagator is equal to zero.

It is of interest to investigate the high temperature or  $\lim_{\beta \rightarrow 0}$  limit of Eq. (2.13). Because  $\lim_{\beta \rightarrow 0} G(\mathbf{r}, \mathbf{r}', \beta) = \delta(\mathbf{r} - \mathbf{r}')$ ,  $\mathbf{r} \rightarrow \mathbf{r}', \chi \rightarrow 0$ , and  $D \rightarrow 4(r-a) \times (r'-a)$ . Thus the factor  $\exp(-D/2\lambda^2)$  is nonvanishing only when  $r \rightarrow a, r' \rightarrow a$ . In this case,  $a(u-a)/rr' \rightarrow 1$ . Thus in the high temperature limit Eq. (2.13) reduces to

$$G(\mathbf{r}, \mathbf{r}', t) = \left(\frac{1}{i2\pi\lambda^2}\right)^{3/2} e^{i(r-r')^2/2\lambda^2} [1 - e^{i2(r-a)(r'-a)/\lambda^2}] \tag{2.14}$$

which is exactly the old image approximation.<sup>2</sup>

$G(r, r', t)$  describes the relative motion of the point particle with respect to the hard sphere. It is easy to transform this into the propagator for the relative motion of two hard spheres of diameters  $\sigma_1$  and  $\sigma_2$  such that  $a = \sigma_1 + \sigma_2$  and masses  $m_1$  and  $m_2$  such that  $m = m_1 m_2 / (m_1 + m_2)$  where  $m$  is now the reduced mass of the pair. Since this gives only the relative motion we must multiply this propagator by a free particle propagator for the center of mass motion. This approach can be used to determine the short time propagator of a system of  $N$  hard spheres.

### III. THE PROPAGATOR INSIDE A HARD SPHERICAL CAVITY

The derivation for the hard sphere propagator can be easily generalized to the case of a particle confined inside a hard spherical cavity. Since the system is bounded the energy eigenvalues are discrete. Thus the integrals of the last section are replaced by summations and the summations can be evaluated using the Poisson summation formula. The Green function can be expressed in terms of eigenvalues and eigenfunctions, that is

$$G(\mathbf{r}, \mathbf{r}', t) = \sum_{l=1}^{\infty} \frac{2l+1}{4\pi} P_l(\cos \chi) I(r, r', l), \tag{3.1}$$

where the angular part is similar to that of Eq. (2.6), and the radial part is given by

$$I(r, r', l) = \sum_{n=0}^{\infty} \frac{1}{N} j_l(x) j_l(x') e^{-i(\lambda k_{n,l})^2/2}, \tag{3.2}$$

where  $x = k_{n,l} r, x' = k_{n,l} r'$ , and  $k_{n,l}$  is the  $n$ th eigenvalue of the  $l$ th spherical Bessel function and  $N$  is the normalization factor. At the limit of  $k_{n,l} a, x, x' \gg 1$ , we can employ the asymptotic formulas for the spherical Bessel functions. Therefore,

$$j_l(x) = \sin\left(x - \frac{l\pi}{2}\right) / x, \tag{3.3}$$

where the eigenvalues are given by

$$k_{n,l} = \frac{\pi}{a} \left(n + \frac{l}{2}\right) \tag{3.4}$$

and the normalization factor is

$$N = \frac{a}{2k_{n,l}^2}. \tag{3.5}$$

Hence, we are able to express function  $I$  in Eq. (3.2) as

$$I(r, r', l) = \sum_{n=0}^{\infty} \frac{2k_{n,l}^2}{a} \frac{1}{xx'} \sin(x - l\pi/2) \times \sin(x' - l\pi/2) e^{-i(k_{n,l})^2/2}. \quad (3.6)$$

Under the assumption that the main contribution of the summation over  $n$  comes from large  $k_{n,l}$  or  $n$ , we can extend the summation of positive integers to that of all integers and obtain

$$I(r, r', l) = \sum_{n=-\infty}^{\infty} \frac{1}{2a} \frac{1}{rr'} [e^{ik_{n,l}(r-r')} - (-1)^l e^{ik_{n,l}(r+r')}] e^{-i(k_{n,l})^2/2}. \quad (3.7)$$

The above expression can be justified by the fact that for  $\lambda \rightarrow 0$  it gives the delta function which is the initial condition of the Green function.

After applying the Poisson summation to Eq. (3.7), we have

$$I(r, r', l) = \frac{1}{2rr'} \sum_{\nu=-\infty}^{\infty} e^{-i\nu\pi l} \sqrt{\frac{2\pi}{i(\pi\lambda)^2}} \times [e^{i(1/2\lambda^2)(r-r'+2\nu a)^2} - (-1)^l e^{i(1/2\lambda^2)(r+r'+2\nu a)^2}], \quad (3.8)$$

where  $\nu$  is the winding number.

Eq. (2.3) allows us to transform Eq. (3.1) with Eq. (3.8) from the spherical coordinates back to Cartesian coordinates. Then, the Green function can be written as

$$G(r, r', t) = \sum_{\nu=-\infty}^{\infty} G_{\nu}(r, r', t), \quad (3.9)$$

where  $G_{\nu}(r, r', t)$  is discussed for different value of  $\nu$ .

For convenience assume  $r \geq r'$ . When  $\nu = 0$ ,

$$G_0(r, r', t) = \left(\frac{1}{2\pi i \lambda^2}\right)^{3/2} e^{i(r-r')^2/2\lambda^2} \quad (3.10)$$

when  $\nu$  is even but nonzero,

$$G_{\nu}(r, r', t) = \left(\frac{1}{2\pi i \lambda^2}\right)^{3/2} \frac{r_{\nu}}{r} e^{i(r_{\nu}-r')^2/2\lambda^2} \quad (3.11)$$

and when  $\nu$  is odd,

$$G_{\nu}(r, r', t) = \left(\frac{1}{2\pi i \lambda^2}\right)^{3/2} \frac{r_{\nu}}{r} e^{i(r_{\nu}+r')^2/2\lambda^2} \quad (3.12)$$

where  $r_{\nu}$  is the  $\nu$ th image of vector  $r$ , and is defined as

$$r_{\nu} = (r + 2\nu a) \hat{e}_r. \quad (3.13)$$

Thus we can write

$$G_{\nu}(r, r', t) = \left(\frac{1}{2\pi i \lambda^2}\right)^{3/2} \frac{r_{\nu}}{r} e^{i[r_{\nu} - (-1)^{\nu} r']^2/2\lambda^2}. \quad (3.14)$$

In a confined system quantum waves are multiply reflected by the boundary. The winding number indicates the number of reflections. When one of the coordinates lies on the hard sphere surface,  $r = a$ , the  $\nu = 0$  and  $\nu = -1$  terms cancel each other. In general, any pair of terms that satisfy  $\nu_1 + \nu_2 = -1$  cancel each other. This one-to-one correspondence eventually cancels all terms with the consequence that the Green function vanishes at the boundary. Thus Eq. (3.14) satisfies the proper boundary condition.

## IV. SIMULATIONS

To test the accuracy of the hard sphere propagator Eq. (2.13) derived in Sec. II, we calculate the radial distribution function of a quantum hard sphere at finite temperatures. This distribution function is important in evaluating the second virial coefficient. It has been calculated by Larsen<sup>9</sup> making use of basis-set expansion techniques. His data allow the calibration of the results of simulations. It has also been calculated by Jacucci and Omerti<sup>3</sup> using imaginary-temperature PIMC simulations, and earlier, by Whitlock and Kalos<sup>7</sup> using Green function Monte Carlo. Both of these calculations are based on use of the image approximation of Eq. (2.14). These simulation results indicated that the image approximation is a great improvement over the free particle propagator, as expected.

Introducing the relative density

$$\rho(r, r', \beta) = \frac{K(r, r', \beta)}{K^0(r, r', \beta)}, \quad (4.1)$$

where  $K$  is the density matrix for a hard sphere and  $K^0$  is the density matrix for a free particle,  $K$  can be expressed as the limit of discretized path integrals,

$$K(r, r', \beta) = \lim_{P \rightarrow \infty} \prod_{i=1}^{P-1} \int dr_i \prod_{i=0}^{P-1} \bar{G}\left(r_i, r_{i+1}, \frac{\beta}{P}\right), \quad (4.2)$$

where  $\bar{G}$  is the imaginary time propagator defined as

$$\bar{G}\left(r, r', \frac{\beta}{P}\right) = G\left(r, r', -i\frac{\beta\hbar}{P}\right) \quad (4.3)$$

and the free particle propagator is

$$\bar{G}(r, r', \beta) = \left(\frac{1}{2\pi\lambda^2}\right)^{3/2} e^{-[(r-r')^2/2\lambda^2]}. \quad (4.4)$$

We can apply either the new hard sphere propagator Eq. (2.13) or the image approximation Eq. (2.14) here.

In Monte Carlo simulations,  $P$  is the discretization parameter. The convergence of the relative density,  $\rho$ , as a function of  $P$  will differ for different propagators and will give a measure the accuracy of the propagator  $\bar{G}$  we use.

Consider the case of two particles interacting with a hard sphere potential. The vector  $r$  is the relative displacement between the two particles. And the direct and exchange

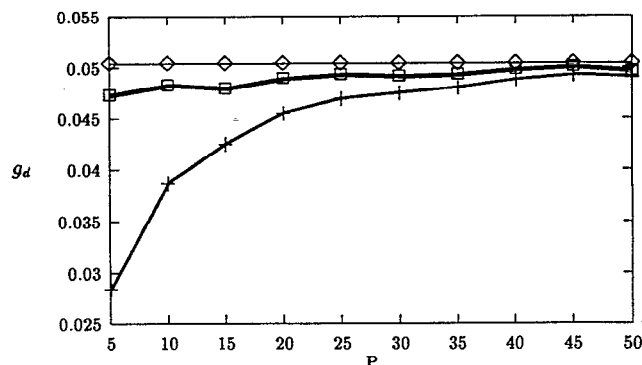


FIG. 1.  $g_d$  of Eq. (4.5) at  $r = 1.25$  and  $\lambda = 5.6$  as a function of the number of beads  $P$ . (a) ◇, the exact result; (b) □, the result for the new propagator Eq. (2.13); (c) +, the result for the image propagator Eq. (2.14).

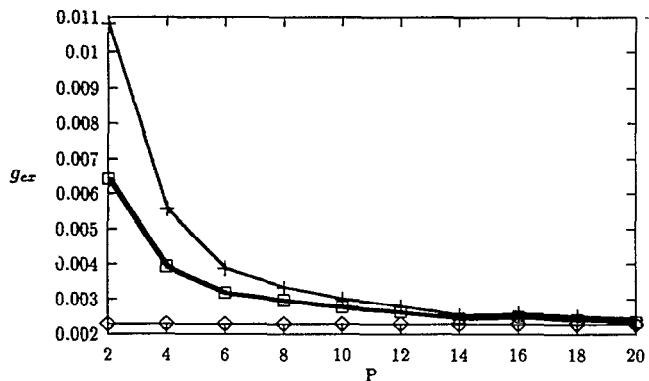


FIG. 2.  $g_{ex}$  of Eq. (4.6) at  $r = 1.25$  and  $\lambda = 1.65$  as a function of the number of beads  $P$ . (a)  $\diamond$ , the exact result; (b)  $\square$ , the result for the new propagator Eq. (2.13); (c)  $+$ , the result for the image propagator Eq. (2.14).

contributions to the two body pair correlation function are defined as

$$g_d(r) = \rho(\mathbf{r}, \mathbf{r}, \beta) \quad (4.5)$$

and

$$g_{ex}(r) = e^{(-2r^2/\lambda^2)} \rho(\mathbf{r}, -\mathbf{r}, \beta), \quad (4.6)$$

so that

$$g(r) = g_d(r) \pm g_{ex}(r). \quad (4.7)$$

At low density this function gives the virial coefficient for boson and fermion particles.

Monte Carlo simulations using a staging technique are used to generate a sequence of  $10^5$  configurations using the new propagator and for comparison purposes using the image approximation. In Fig. 1  $g_d(r)$  is plotted as a function of  $P$  for  $r = 1.25$  and  $\lambda = 5.6$  (in units of the hard sphere radius). In Fig. 2 the exchange term  $g_{ex}(r)$  is plotted as a function of  $P$  for the same parameters.

For a particle inside a spherical cavity,<sup>5</sup> we define the distribution function as

$$g_d(r) = \rho(\mathbf{r}, \mathbf{r}, \beta). \quad (4.8)$$

Monte Carlo simulations using a staging technique are used to generate a sequence of  $10^5$  configurations using the new propagator Eq. (3.9) and for comparison purposes using the image approximation. The new propagator Eq. (3.9) is used with summation of the two terms  $\nu = 0$  and  $\nu = -1$ . In Fig. 3,  $g_d$  is plotted as a function of  $P$  for  $r = 0.0$  and  $\lambda = 1.0$ .

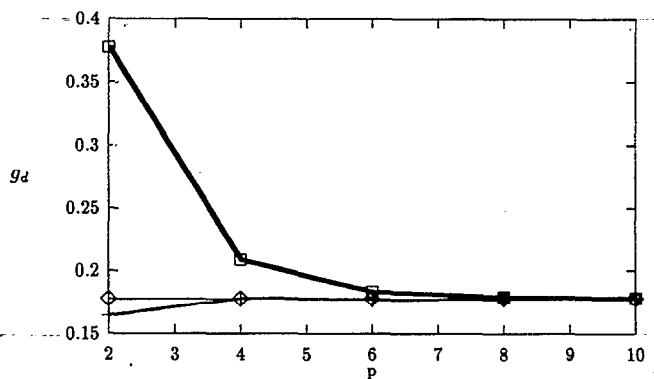


FIG. 3.  $g_d$  of a particle inside a spherical cavity defined by Eq. (4.8) at  $r = 0.0$  for  $\lambda = 1.0$  as a function of the number of beads  $P$ . (a)  $\diamond$ , the exact result; (b)  $+$ , the result for the new propagator Eq. (3.9); (c)  $\square$ , the result for the image propagator Eq. (2.14).

For fixed number of beads  $P$  the addition of terms of higher winding numbers should improve the convergence. It was found here that when terms with  $\nu = 1$  and  $\nu = -2$  are included for  $P > 2$  little was gained from these added terms.

For further application, we can simulate an atom confined in a spherical cavity. Then the propagator is taken as the product of the new propagator Eq. (3.9) and the factor due to the interaction inside the atom

$$\bar{G}\left(\vec{r}, \vec{r}', \frac{\beta}{P}\right) = \prod_{\alpha=1}^n \bar{G}\left[\mathbf{r}_{(\alpha)}, \mathbf{r}'_{(\alpha)}, \frac{\beta}{P}\right] e^{-\beta/2P[U(\vec{r}) + U(\vec{r}')]}, \quad (4.9)$$

where  $n$  is the number of coordinates involved in the atom,  $\vec{r}$  is this set of coordinates  $\vec{r} = [\mathbf{r}_{(1)}, \mathbf{r}_{(2)}, \dots, \mathbf{r}_{(n)}]$  and  $U(\vec{r})$  is the interaction potential between particles.

It is obvious that the new propagators converge much faster than the image approximation and should thus be preferable for simulations of hard sphere and hard cavity systems.

<sup>1</sup>B. J. Berne and D. Thirumalai, *Ann. Rev. Phys. Chem.* **37**, 401 (1986).

<sup>2</sup>J. Barker, *J. Chem. Phys.* **70**, 2914 (1979).

<sup>3</sup>G. Jacucci and E. Omerti, *J. Chem. Phys.* **76**, 3051 (1983).

<sup>4</sup>M. L. Klein, M. Sprik, and D. Chandler, *Phys. Rev. B* **31**, 4234 (1985).

<sup>5</sup>Z. H. Liu and J. Broughton, *Phys. Rev. B* **40**, 571 (1989).

<sup>6</sup>G. E. Uhlenbeck and E. Beth, *Phys. Fenn.* **3**, 729 (1936).

<sup>7</sup>P. A. Whitlock and M. H. Kalos, *J. Comput. Phys.* **30**, 361 (1979).

<sup>8</sup>J. J. Sakurai (Addison-Wesley, New York, 1985).

<sup>9</sup>S. Y. Larsen, *J. Chem. Phys.* **48**, 1701 (1968).